

COMPUTATIONAL STUDY OF RAREFIED FLOW INSIDE A LID DRIVEN CAVITY USING A MIXED MODAL DISCONTINUOUS GALERKIN METHOD

T. Chourushi,¹ S. Singh¹ and R.S. Myong^{*1,2}

¹Graduate School of Mechanical and Aerospace Engineering, Gyeongsang National University

²Dept. of Aerospace and Software Engineering & ReCAPT, Gyeongsang National University

혼합 Modal 불연속 Galerkin 기법을 이용한 Lid-Driven Cavity 내의 희박유동 전산 연구

투샬 초루시,¹ 사티비르 싱,¹ 명 노 신^{*1,2}

¹경상대학교 대학원 기계항공공학부

²경상대학교 항공우주및SW공학전공 및 항공기부품기술연구소

With the advancement of fabrication technology and miniaturization, fluid flows at micro- and nano-scales has received considerable attention. Flow characteristics in these systems significantly vary from those of macro- scale devices, due to geometric restrictions. In such cases, Navier-Stokes-Fourier(NSF) equations with no-slip condition may not be valid for studying gas flows inside a micro- cavity. This article therefore investigates the cavity flows using modified NSF equations with velocity slip and temperature jump conditions. In the present case, a monatomic gas is considered for modelling gas flows. To accurately predict the flow physics, mixed modal discontinuous Galerkin(DG) method is being developed. The flow characteristics of monatomic gas is studied by varying the Reynolds number(Re) and Knudsen number(Kn), respectively. Results obtained are compared with the previous results and are found to be in good agreement with them.

Key Words : Micro-fluidics, cavity flows, discontinuous Galerkin method, rarefied gas

1. Introduction

Industrial, commercial and governmental research organizations are constantly working on miniaturization of devices to satisfy the consumer needs. These devices include hard-disk drive heads, ink-jet printer heads, micro heat-exchangers, micro pumps, and turbines. The gas flow under these micro-systems significantly varies from that of conventional (macro-systems) devices, as the characteristic length reduces to few microns. Under such circumstances, Navier-Stokes-Fourier(NSF) equations with no-slip

boundary conditions may not remain valid, as the flow enters into non-equilibrium conditions[1,2]. In the past, several studies have been conducted to prove the inability of NSF equations with no-slip boundary conditions to study micro- fluids[3-5].

At micro scales, number of intermolecular collisions are significantly reduced, and thus non-equilibrium effects start to dominate[4]. This degree of rarefaction of a gas is defined with the Knudsen number(Kn). To describe the rarefied gas, the Boltzmann transport equation(BTE) is consequently considered as the fundamental equation. In the past, several methods have been devised to solve these equations, out of which Direct Simulation of Monte Carlo (DSMC) method is often used for numerical simulation of BTE[6]. However, DSMC is subject to high statistical noise at low flow speeds, which is a typical situation for micro gases. Also, DSMC is computationally expensive in

Received: August 10, 2018, Revised: September 25, 2018,

Accepted: September 25, 2018.

* Corresponding author, E-mail: myong@gnu.ac.kr

DOI <http://dx.doi.org/10.6112/kscfe.2018.23.3.062>

© KSCFE 2018

nature[7]. To overcome these shortcoming, NSF equations with velocity slip and temperature jump boundary conditions are considered due to its ability to predict non-equilibrium effects. These modified equations are hereafter called as modified NSF equations in rest of this paper. Until now, very few studies have been presented to study cavity flows using modified NSF equations[4], which is the main objective of this study.

Among the existing numerical methods, discontinuous Galerkin(DG) method is often considered to compute low Mach number flow problems as it does not require time-preconditioning techniques, which are often required in finite volume method(FVM)[8]. The essential idea of the DG method is derived from the shape functions which are considered discontinuous across the element boundaries. This feature enables it to avoid the need of assembling global matrix leading to less in-core memory required in computation when compared with continuous Galerkin method[9]. Although the DG method looks attractive, it was considered difficult to implement for NSF equations, until Bassi and Rebay[10] presented a novel approach, called as “mixed” DG method. Till date, no works based on explicit mixed modal DG method for the modified NSF equations is being reported for low-Mach gas flow inside a lid-driven cavity.

In this study, we aim to investigate the rarefied monatomic gas flow inside a lid-driven cavity. For this purpose, a high order mixed modal discontinuous Galerkin method is employed to solve the two-dimensional conservation laws. In the present work, we studied the effect of Reynolds number(Re) and Kn on the flow characteristics of cavity flows. To verify these results, comparison with the literature is also presented.

2. Mathematical Formulation and Numerical Procedure

2.1. Problem definition

Figure 1 presents a schematic diagram of the lid-driven cavity. The computational domain is set to be a square with $x=L$ and $y=L$. The top wall of the cavity moves with a constant velocity (50 m/s) in x direction. The other wall boundaries at $x=0$ and $x=L$ and $y=0$ are assumed stationary. All the walls are considered to be isothermal, with a temperature $T_w = 273\text{ K}$.

Here we consider monatomic rarefied argon gas confined in the geometry with a shear viscosity index of 0.81. In all simulations, the Knudsen number Kn ranges from 0.000259 to 0.05, which is expressed as:

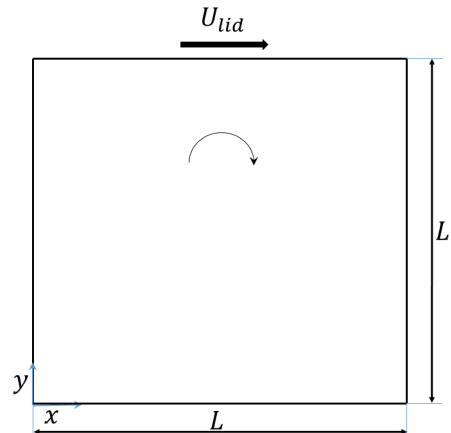


Fig. 1 Schematic diagram of lid-driven square cavity

$$Kn = \frac{M}{Re} \sqrt{\frac{\gamma\pi}{2}} \tag{1}$$

The current work details the study of both continuum and non-continuum flows. In case of continuum flows, three values of Re (based on the corresponding Kn for a given Mach number) are considered, i.e., $Re = 100, 400$ and 1000 . For the case of non-continuum flows, three values of Kn are studied, i.e., $Kn = 0.00259, 0.0259$ and 0.05 .

Additionally, we also performed a grid study to find computationally efficient mesh characteristics. All numerical simulations are performed with the specified top wall boundary condition for a constant moving velocity field in the x direction. This velocity field is calculated in reference to low Mach number $M = 0.16$. The cavity presented is subjected to partial slip boundary condition which is imposed on these walls[11]. In all simulations, flow is assumed to be unsteady and laminar.

2.2. Governing equations for monatomic gas

The Boltzmann kinetic equation for monatomic gas particles can be expressed as, in case of no external field,

$$\left(\frac{\partial}{\partial t} + \mathbf{v} \cdot \nabla \right) f(\mathbf{v}, \mathbf{r}, t) = R[f] \tag{2}$$

where f , \mathbf{v} , \mathbf{r} , and $R[f]$ represent the distribution function, the particle velocity, the particle position, and the collision integral, respectively[12]. In reference to gas kinetic theory, there are two different sets of macroscopic variables including the conservative variables (ρ, \mathbf{u}, E) and

the non-conservative variables, viscous shear stresses and heat fluxes, $(\mathbf{\Pi}, \mathbf{Q})$. These variables can be represented by a statistical formula

$$\Phi^{(k)} = \langle h^{(k)} f \rangle \quad (3)$$

where the angular bracket denotes the integration over the variable \mathbf{v} . The $h^{(k)}$ indicates the molecular expressions for moments. The leading elements of the set of the conservative variables and non-conservative variables are defined as

$$\Phi^{(1)} = \rho, \quad \Phi^{(2)} = \rho \mathbf{u}, \quad \Phi^{(3)} = \rho E, \quad (4)$$

$$\Phi^{(4)} = \mathbf{\Pi} = [\mathbf{P}]^{(2)}, \quad \Phi^{(5)} = \mathbf{Q}.$$

with the molecular expressions corresponding to this set

$$h^{(1)} = m, \quad h^{(2)} = m \mathbf{v}, \quad h^{(3)} = \frac{1}{2} m C^2, \quad (5)$$

$$h^{(4)} = [m \mathbf{c} \mathbf{c}]^{(2)}, \quad h^{(5)} = \frac{1}{2} m C^2 - m \hat{h}.$$

Here ρ is the density, \mathbf{u} is the average velocity vector, E is the total energy density, p is the pressure, m is the molecular mass, \mathbf{c} denotes the peculiar velocity of the molecule, and \hat{h} represents the enthalpy density per unit mass. The symbol $[]^{(2)}$ denotes the traceless symmetric part of the second rank tensor. The shear stresses are related to the stress tensor \mathbf{P} through the relation

$$\mathbf{P} = p \mathbf{I} + \mathbf{\Pi} \quad (6)$$

where \mathbf{I} is the unit second rank tensor. The expressions (5) are collision invariants and there is no dissipation term for the conserved variables. Thus the kinetic equation (2) can be derived into a set of evolution equations of conserved variables according to the conservation laws as follow,

$$\frac{\partial}{\partial t} \begin{bmatrix} \rho \\ \rho \mathbf{u} \\ \rho E \end{bmatrix} + \nabla \cdot \begin{bmatrix} \rho \mathbf{u} \\ \rho \mathbf{u} \mathbf{u} + p \mathbf{I} \\ (\rho E + p) \mathbf{u} \end{bmatrix} + \nabla \cdot \begin{bmatrix} 0 \\ \mathbf{\Pi} \\ \mathbf{\Pi} \cdot \mathbf{u} + \mathbf{Q} \end{bmatrix} = 0. \quad (7)$$

The equation (7) can be written in non-dimensional vector form using proper dimensionless variables and parameters as [12],

$$\frac{\partial \mathbf{U}}{\partial t} + \nabla \cdot \mathbf{F}_{inv}(\mathbf{U}) + \nabla \cdot \mathbf{F}_{vis}(\mathbf{U}, \nabla \mathbf{U}) = 0. \quad (8)$$

where the conservative vector \mathbf{U} , the inviscid flux vector \mathbf{F}_{inv} and the viscous flux vector \mathbf{F}_{vis} are given by

$$\mathbf{U} = \begin{bmatrix} \rho \\ \rho \mathbf{u} \\ \rho E \end{bmatrix}, \quad \mathbf{F}_{inv} = \begin{bmatrix} \rho \mathbf{u} \\ \rho \mathbf{u} \mathbf{u} + \frac{1}{\gamma M^2} p \mathbf{I} \\ \left(\rho E + \frac{1}{\gamma M^2} p \right) \mathbf{u} \end{bmatrix}, \quad (9)$$

$$\mathbf{F}_{vis} = \frac{1}{Re} \begin{bmatrix} 0 \\ \mathbf{\Pi} \\ \mathbf{\Pi} \cdot \mathbf{u} + \frac{1}{Ec Pr} \mathbf{Q} \end{bmatrix}.$$

Here the dimensionless numbers, Mach (M), Reynolds (Re), Eckert (Ec) and Prandtl (Pr), can be defined as

$$M \equiv \frac{u_r}{\sqrt{\gamma R T}}, \quad Re \equiv \frac{\rho_r u_r L}{\mu_r}, \quad (10)$$

$$Ec \equiv (\gamma - 1) M^2, \quad Pr \equiv \frac{C_p \mu_r}{k_r},$$

where the subscript r stands for the reference state, γ is the specific heat ratio, T is the temperature, R is the gas constant, and C_p is the reference heat capacity per mass at constant pressure.

For the classical Navier-Stokes-Fourier model, the stress tensor $\mathbf{\Pi}$ and the heat flux vector \mathbf{Q} are computed by the Newtonian law of shear and the Fourier law of heat conduction, respectively, as follows,

$$\mathbf{\Pi} = -2\mu [\nabla \mathbf{u}]^{(2)}, \quad \mathbf{Q} = -k \nabla T, \quad (11)$$

where μ and k are the Chapman-Enskog viscosity, and the thermal conductivity, respectively, for the monatomic molecule and can be expressed as,

$$\mu = T^s, \quad k = T^s \text{ and } s = \frac{1}{2} + 2/(\nu - 1). \quad (12)$$

The ν denotes the exponent of the inverse power laws for the gas particle interaction potentials[8].

2.3. Discontinuous Galerkin formulation

The computational domain is discretized using the

mixed modal DG method in reference to Bassi and Rebay[10] formulation. This formulation determines the value of the second-order derivatives present in viscous terms by adding auxiliary unknowns \mathcal{S} , because the second-order derivatives cannot be accommodated directly in a weak formulation using a discontinuous function space. Therefore, \mathcal{S} can be defined as the derivative of either primitive or conservative variables \mathbf{U} . Hence, equation (7) can be reformulated as the coupled system for \mathcal{S} and \mathbf{U} as

$$\frac{\partial \mathbf{U}}{\partial t} + \nabla \cdot \mathbf{F}_{inv}(\mathbf{U}) + \nabla \cdot \mathbf{F}_{vis}(\mathbf{U}, \mathcal{S}) = 0, \quad (13)$$

$$\mathcal{S} - \nabla \mathbf{U} = 0.$$

These equations refer to a coupled system of equations in which the computational domain is decomposed into unstructured triangular elements. The exact solutions of \mathbf{U} and \mathcal{S} are approximated by the DG polynomial approximations of \mathbf{U}_h and \mathcal{S}_h , respectively.

$$\begin{aligned} \mathbf{U}_h &= \sum_{i=0}^{N_k} u_h^i(t) \phi^i(\mathbf{x}), \\ \mathcal{S}_h &= \sum_{i=0}^{N_k} s_h^i(t) \phi^i(\mathbf{x}), \quad \forall \mathbf{x} \in \Omega_e. \end{aligned} \quad (14)$$

where $u_h^i(t)$ and $s_h^i(t)$ are the local degrees of freedom of \mathbf{U} and \mathcal{S} , $\phi^i(\mathbf{x})$ is the basis functions for finite element space, and N_k is the number of required basis function for the k -exact DG approximation. In the present work, second order of Dubiner basis functions and third order explicit DG scheme are adopted for triangular elements. The mixed system (13) is multiplied with the test function, which is taken to be equal to the basis function $\phi^i(\mathbf{x})$, and then integrated by parts over an element Ω_e . This results in the weak formulation of the mixed system for \mathbf{U}_h and \mathcal{S}_h ,

$$\begin{aligned} \frac{\partial}{\partial t} \int_{\Omega_e} \mathbf{U}_h \phi^i dV - \int_{\Omega_e} \nabla \phi \cdot \mathbf{F}_{inv} dV - \int_{\Omega_e} \nabla \phi \cdot \mathbf{F}_{vis} dV \\ + \int_{\partial \Omega_e} \phi \mathbf{F}_{inv} \cdot \mathbf{n} d\Gamma + \int_{\partial \Omega_e} \phi \mathbf{F}_{vis} \cdot \mathbf{n} d\Gamma = 0, \\ \int_{\Omega_e} \mathcal{S}_h \phi^i dV + \int_{\Omega_e} \nabla \phi \mathbf{U}_h dV - \int_{\partial \Omega_e} \phi \mathbf{U}_h \cdot \mathbf{n} d\Gamma = 0, \end{aligned} \quad (15)$$

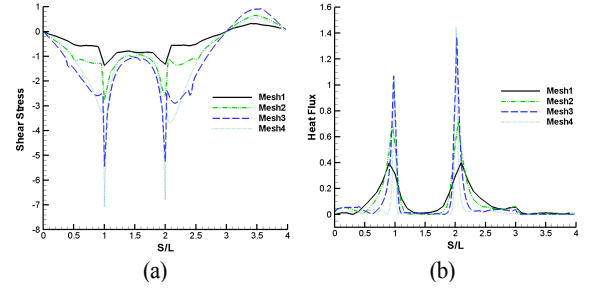


Fig. 2 Comparison of shear stress and heat flux along the walls of cavity for different meshes, at $Kn = 0.000647$ and $Ma = 0.16$

where \mathbf{n} is the outward normal vector, V and Γ denote the volume and boundary of the element, respectively. In the above formulation, the Gaussian-Legendre quadrature rule has been implemented for both boundary and volume integrations. Therefore, the volume and boundary integrals in equation (15) are computed using $2k$ and $2k+1$ order accurate Gauss quadrature formulas, respectively[8]. Three quadrature points on edges and 5 quadrature points inside the elements are used for boundary and volume integrations. In this work, we considered local Lax-Friedrichs and BR1 schemes for inviscid and viscous terms, respectively. In order to limit the spurious numerical fluctuations in the solutions for higher order schemes, positivity preserving limiter is used. A third-order total variation diminishing Runge-Kutta(TVD-RK) method is employed for explicit time marching[13]. Furthermore, in order to simulate gas-solid slip, the maxwell velocity and temperature slip/jump conditions[14] are considered.

3. Grid Study and Verification of the Code

In this section, we describe the grid independency and verification studies for the code in reference to argon gas.

3.1. The grid independency test

In order to minimize the computational cost, simulations are carried out using four grid resolutions Mesh1=40($\times 4$, walls), Mesh2=80($\times 4$), Mesh3=160($\times 4$) and Mesh4=320($\times 4$) for unstructured triangular elements. To ensure grid independence, distributions of the shear stresses and heat fluxes along wall boundaries are investigated. Figure 2 shows the comparison of shear stress and heat flux, along the walls of the cavity for different meshes, at $Re = 400$, $Kn = 0.000647$ and $Ma = 0.16$. In these figures, it has been observed that the

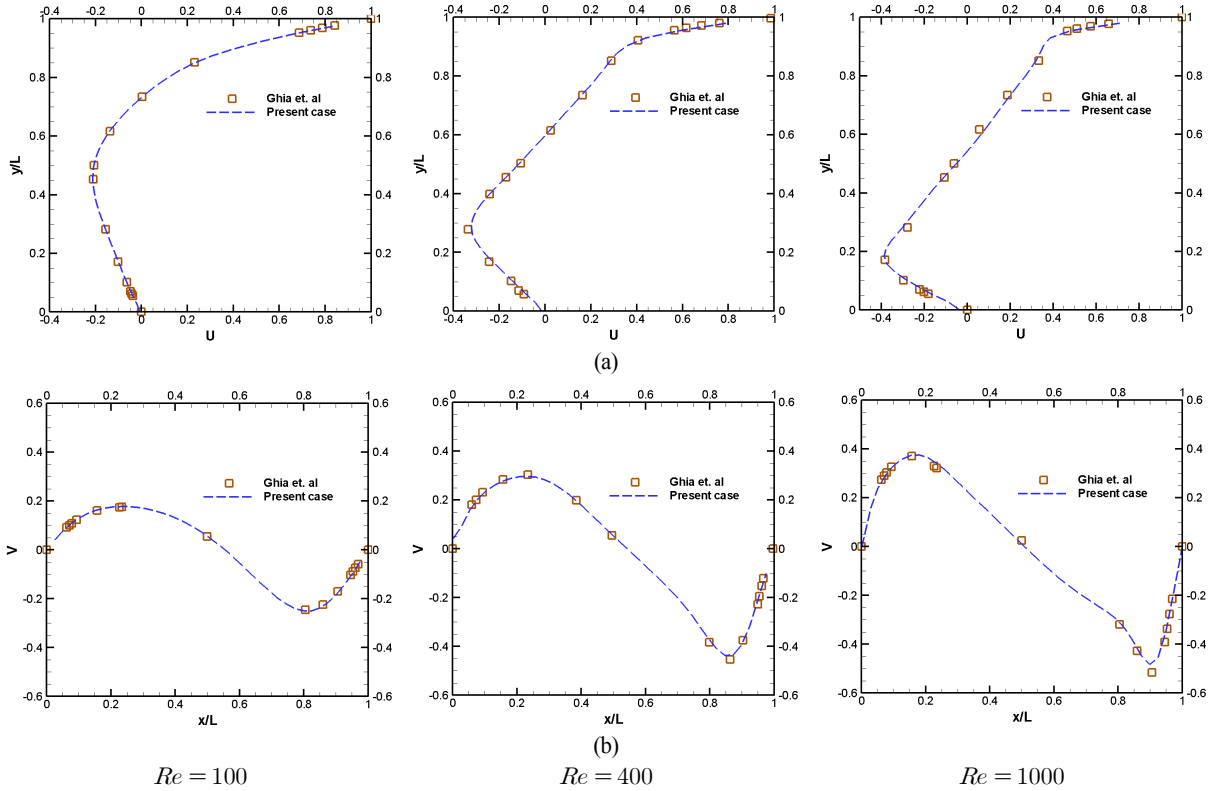


Fig. 3 Comparison of profiles: (a) “u” velocity along the vertical central line (y/L), and (b) “v” velocity along the horizontal central line (x/L), at $Re = 100, 400, 1000$

simulation errors for coarse grids are more pronounced on the moving lid. This can be attributed due to the presence of higher gradients on the moving lid when compared to the stationary walls. In all, both Mesh3 and Mesh4 performed similar. However for computational efficiency, grid resolution of Mesh3=160(\times 4) is considered in the present case. All numerical simulations are performed with Courant-Friedrichs-Lewy(CFL) number of 0.1.

3.2. Verification of the code

For verification of the present work, we first studied flow in the continuum regime and later flow in the non-continuum regime. In case of continuum regime, we compared our results with Ghia et al.[15] for three different Re . The plot of profiles for velocity field in x - and y - directions along central line of the cavity are considered. Figure 3 outlines the comparison of “u” and “v” velocity components along the vertical and horizontal central lines of the cavity, at $Re = 100, 400$ and 1000 . Based on these plots, it can be found that our results are

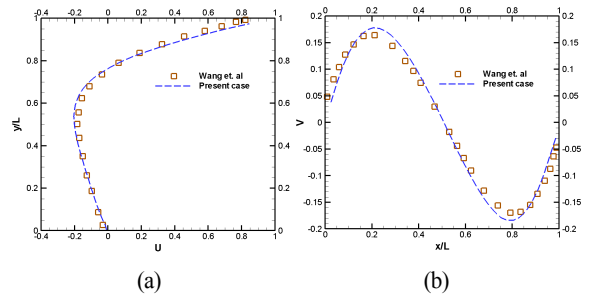


Fig. 4 Comparison of profiles: (a) “u” velocity along the vertical central line (y/L), and (b) “v” velocity along the horizontal central line (x/L), at $Kn = 0.0259, Re = 10$

in good agreement with previous results in the literature. For the case of non-continuum regime, we compared the velocity profiles with Wang et al.[16], for argon gas at $Kn = 0.0259$ and $Re = 10$, as shown in Fig. 4. Fairly good agreement with previous results is obtained from these plots.

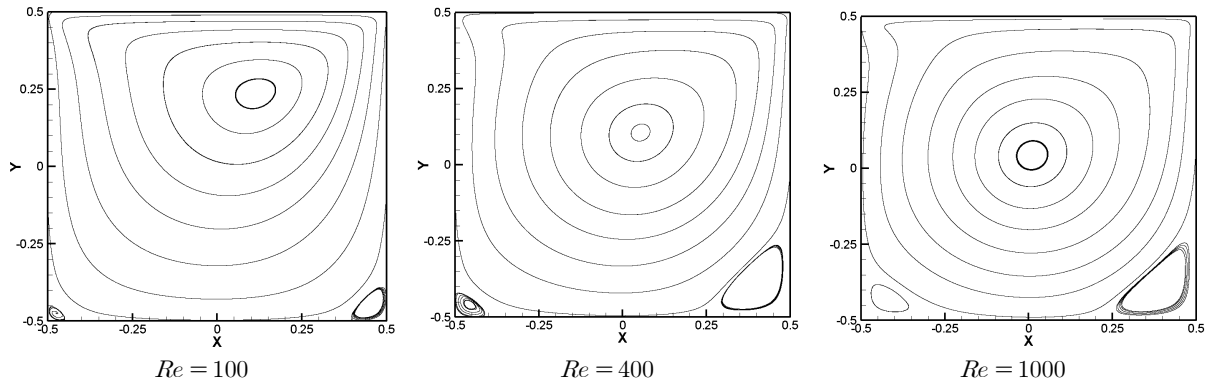


Fig. 5 Streamline plots of lid-driven cavity at different Re : (a) 100, (b) 400 and (c) 1000, for $M = 0.16$

4. Results and Discussion

In this section, numerical simulations for the two-dimensional(2D) lid-driven cavity are presented. In the first part, near-equilibrium flows are simulated and compared. In the second part, rarefied flow using modified NSF equations are computed.

4.1. Effect of Reynolds number on cavity flows

Three cases are selected to explain the effect of the Reynolds numbers: $Re = 100, 400$ and 1000 for same Mach number, $M = 0.16$. In these simulations, the wall velocity is kept fixed i.e., $U_w = 50 \text{ m/s}$. Depending upon the Re , Kn is varied in reference to equation (1). In all simulations, $CFL = 0.1$ is taken for numerical convergence. Initial temperature of argon gas is assumed to be same as the wall temperature ($T_w = 273.15 \text{ K}$). The variable hard sphere (VHS) model is considered for molecular collisions and viscosity index is set to 0.81.

Figure 5 shows the streamline plot for lid-driven cavity at different Re . The distributions illustrate that both primary and secondary vortices are efficiently captured. Also it has been noticed that as the Re increase, the centre of primary vortex shift towards the centre of cavity and secondary vortices gain strength which is in agreement with the previous results, Ghia et al.[15]. Also, it has been observed that as the $Re = 1000$, tertiary vortex appears at the top left corner of the cavity. These plots clearly agree with the plots of velocity profiles as shown in Fig. 3.

Figure 6 shows the comparison of contour plots of flow variables i.e., “u” velocity, mach number, pressure and temperature fields, for the lid-driven cavity based on

different Re , at $Ma = 0.16$. These plots clearly show that as the Re increases, distinct primary vortex is formed at the centre of the cavity. Also it is observed that the temperature distribution remains isothermal across the stationary walls. However, in the vicinity of moving wall, higher temperature gradients are noticed due to constant moving wall and high pressure gradients. In general, it is noted that the expansion cooling does not occur in these tests, as $T \approx T_w$ in almost the entire region. Thus, viscous dissipation governs the overall heat transfer mechanism. Moreover, it has been found that the Re significantly affect the temperature distribution. As the value of Re increase, low temperature field is obtained at the centre of cavity which is apparently absent at $Re = 100$.

4.2. Effect of Knudsen number on cavity flows

In this part, we consider three test cases to investigate the effect of Knudsen numbers: $Kn = 0.00259, 0.0259$ and 0.05 for the gas at $M = 0.16$. In these simulations, the wall velocity is kept fixed i.e., $U_w = 50 \text{ m/s}$. And CFL number is set to 0.1. Initial temperature of gas is assumed to be same as the wall temperature ($T_w = 273.15 \text{ K}$). The variable hard sphere(VHS) model is considered for molecular collisions and viscosity index is set to 0.81.

Figure 7 shows the comparison of velocity profiles along central lines of the cavity at $Kn = 0.0259$, with Wang et al.[16]. As detailed in these plots, velocity field closely follows the literature. In the Fig. 7, comparison of contour plots of velocity, Mach number, pressure and temperature fields are presented for NSF and modified NSF equations. In these plots, no major difference is observed between the contour plot of velocity and Mach

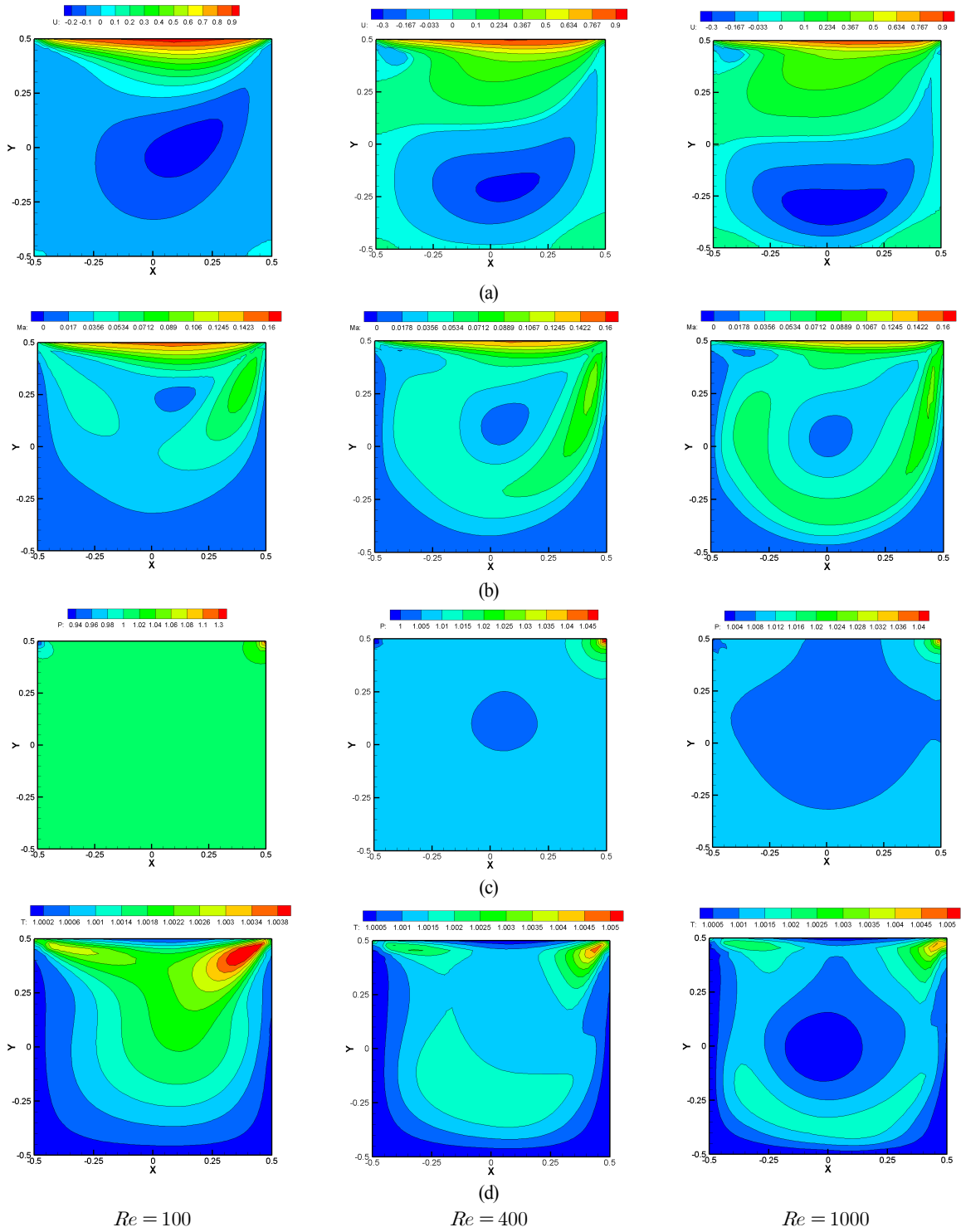


Fig. 6 Contour plots of flow variables: (a) “u” velocity, (b) Mach number, (c) pressure, and (d) temperature, for lid-driven cavity at different Re and $M = 0.16$

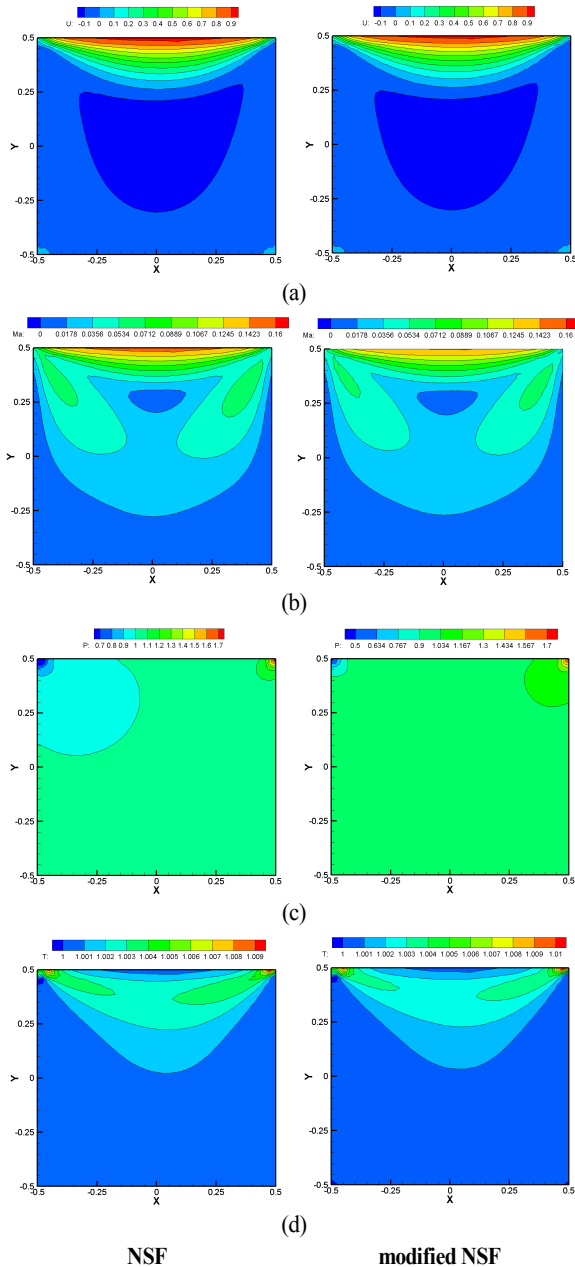


Fig. 7 Comparison of contour plots: (a) “u” velocity, and (b) Mach number, (c) pressure, and (d) temperature, for NSF and modified NSF equations for cavity flows, at $Kn = 0.0259$, $Re = 10$

number. In case of the modified NSF equations, low pressure region on the top-left corner of the cavity is efficiently captured which is absent for the NSF equations. In case of slip, gas density reduces near the top-left

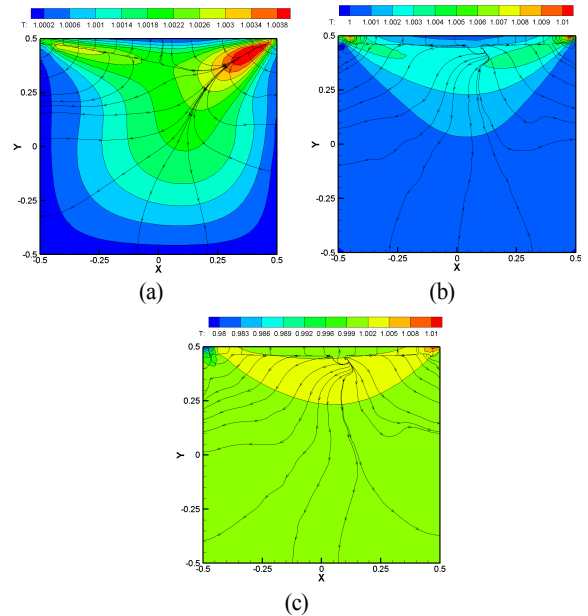


Fig. 8 Comparison of heat flux stream traces overlaid on temperature contours (K) for the cavity, at different Kn : (a) 0.00259, (b) 0.0259, and (c) 0.05

corner of the cavity which gives rise to low pressure region. By incorporating slip condition, this behavior is well captured. Also, the contour plots of temperature field slightly differ for the NSF and modified NSF equations. In general the NSF equation under-predicts the temperature field when compared with the modified NSF equation.

In order to further evaluate this difference for non-continuum flows, the plot of heat flux stream traces overlaid on temperature contour is illustrated in Fig. 8. The results show that the trend in the temperature field is from hot to cold regions. In case of low Kn (i.e., $Kn = 0.00259, 0.0259$) flows, $T \approx T_W$ in almost the entire region so viscous dissipation dominates the heat transfer mechanism. With the further increase in Kn (i.e., $Kn = 0.05$), both expansion cooling and viscous dissipation are observed, which governs the heat transfer mechanism for rarefied gas cavity flows. At the top left corner of the cavity, expansion cooling phenomena is noticed, as $T < T_W$, which is almost absent at low Kn .

In Fig. 9, “u” and “v” velocity components along vertical and horizontal central lines of the cavity are presented, respectively for $Kn = 0.00259$ and 0.0259. For flow near to continuum regime (i.e., $Kn = 0.00259$), “v” velocity component is close to zero at both left and right stationary walls of the cavity. However, for

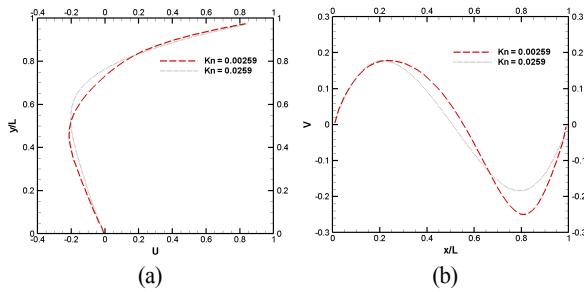


Fig. 9 Comparison of profiles: (a) “ u ” velocity along the vertical central line (y/L), and (b) “ v ” velocity along the horizontal central line (x/L), at $Kn = 0.00259$ and 0.0259

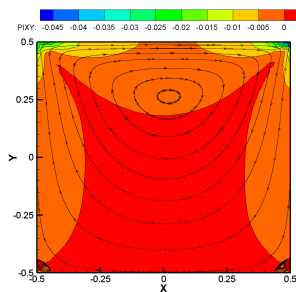


Fig. 10 Comparison of velocity streamlines overlaid on shear stress contours for the cavity ($Kn=0.0259$)

non-equilibrium flows “ v ” velocity slip attains a finite value, as referred in the plots. Also, it has been found that with increasing Kn , the gradients of “ v ” velocity component tends to be smoother.

Finally, Fig. 10 shows the velocity streamlines superimposed on viscous shear stress contours. At this low Re , streamlines are symmetric with respect to the central vertical line of the cavity, which is in agreement with previous literature[17]. Furthermore, in this plot it has been observed that the top corners of the cavity generates maximum shear stress. Also, at this plot the shear stresses are non-symmetric with respect to the central vertical line of the cavity. In general, comparatively high shear stresses are found at the top right corner of the cavity.

5. Conclusion

In this study, the flow characteristics inside a lid-driven square cavity is presented by solving two-dimensional conservation laws for monatomic gas. A high order discontinuous Galerkin method is employed for spatial and time integrals.

The effect of Reynolds number and Knudsen number on the flow and thermal characteristics of a monatomic gas in a lid-driven cavity are discussed in detail. It has been observed that as the Re increase, distinct primary and secondary vortices are formed. Moreover, low temperature field at the centre of cavity is noticed at high Re which is apparently absent at $Re = 100$. In the later case when Kn is varied, it has been found that both the pressure and temperature fields are not well captured by NSF equations. As the Kn increases, smoother profiles are obtained for v -velocity component. For continuum flows, viscous dissipation governs the heat transfer mechanism. Alternatively, for flow under non-equilibrium conditions, it reveals that both expansion cooling and viscous dissipation dictate the heat transfer mechanism.

Acknowledgements

This work was supported by the National Research Foundation of Korea funded by the Ministry of Education, Science and Technology (NRF 2017-R1A2B2007634), South Korea.

References

- [1] 1999, Gad-el-Hak, M, "The fluid mechanics of microdevices - The freeman scholar lecture," *Journal of Fluid Engineering*, Vol.121, pp.5-33.
- [2] 2005, Karniadakis, M., Beskok, A. and Aluru, N., *Microflows and Nanoflows: Fundamentals and Simulation*, Springer-Verlag, New York.
- [3] 2000, Jie, D., Diao, X., Cheong, K.B. and Yong, L.K., "Navier-Stokes simulations of gas flow in micro devices," *Journal of Micromechanics and Microengineering*, Vol.10, pp.372-379.
- [4] 2007, Mizzi, S., Emerson, D.R., Stenov, S.K., Barber R.W. and Reese J.M., "Effects of rarefaction on cavity flow in the slip regime," *Journal of Computational and Theoretical Nanoscience*, Vol.4, pp.817-822.
- [5] 2014, Ismael, M.A., Pop, I. and Chamkha, A.J., "Mixed convection in a lid-driven square cavity with partial slip," *International Journal of Thermal Sciences*, Vol.8, pp.47-61.
- [6] 2010, John, B., Xiao-Jun, Gu. and Emerson D.R., "Investigation of heat and mass transfer in a lid-driven cavity under non-equilibrium flow conditions," *Numerical Heat Transfer, Part B: Fundamentals: An*

- International Journal of Computation and Methodology*, Vol.58, pp.287-303.
- [7] 2005, Naris, S. and Valougeorgis, D., "The driven cavity flow over the whole range of the Knudsen number," *Physics of Fluids*, Vol.17, 097106.
- [8] 2014, Le, N.T.P., Xiao, H. and Myong, R.S., "A triangular discontinuous Galerkin method for non-newtonian implicit constitutive models of rarefied and microscale gases," *Journal of Computational Physics*, Vol.273, pp.160-184.
- [9] 2006, Le, B.Q., *Discontinuous Finite Elements in Fluid Dynamics and Heat Transfer*, Springer, New York.
- [10] 1997, Bassi, F. and Rebay, S., "A high-order accurate discontinuous finite element method for the numerical solution of the compressible Navier-Stokes equations," *Journal of Computational Physics*, Vol.131, pp.267-279.
- [11] 1879, Maxwell, J.C., "On stresses in rarefied gases arising from inequalities of temperature," *Philosophical Transactions of the Royal Society*, Vol.170, pp.231-256.
- [12] 2004, Myong, R.S., "A generalized hydrodynamic computational model for rarefied and microscale diatomic gas flows," *Journal of Computational Physics*, Vol.195, pp.655-676.
- [13] 1998, Cockburn, B. and Shu, C.W., "The Runge-Kutta discontinuous Galerkin method for conservation laws V: multidimensional systems," *Journal of Computational Physics*, Vol.141, pp.199-224.
- [14] 2017, Shu, J.J., Teo, J.B.M. and Chan, W.K., "Fluid velocity slip and temperature jump at a solid surface," *Applied Mechanics Reviews*, Vol.69, 020801-13.
- [15] 1982, Ghia, U., Ghia, N. and Shin, C.T., "High-Resolution solutions for incompressible flow using the Navier-Stokes equations and a multigrid method," *Journal of Computational Physics*, Vol.48, pp.387-411.
- [16] 2018, Wang, P., Ho, M.T., Wu, L., Guo, Z. and Zhang, Y., "A comparative study of discrete velocity methods for low-speed rarefied gas flows," *Computers & Fluids*, Vol.161, pp.33-46.
- [17] 2017, Eskandari, M. and Nourazar, S.S., "On the time relaxed Monte Carlo computations for the lid-driven cavity flow," *Journal of Computational Physics*, Vol.343, pp.355-367.